Publishing House
AKAPIT

COMPUTER METHODS IN MATERIALS SCIENCE

Informatyka w Technologii Materiałów

Vol. 14, 2014, No. 1

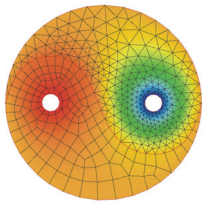

VALIDATION OF MATERIAL MODELS FOR BAINITIC STEELS USED IN OPTIMIZATION OF MANUFACTURING CHAIN FOR FASTENERS

ROMAN KUZIAK[1], KRZYSZTOF RADWAŃSKI[1], KONRAD PERZYŃSKI[2]*, ŁUKASZ MADEJ[2], MACIEJ PIETRZYK[2]

[1]Institute for Ferrous Metallurgy, ul. K. Miarki 12, 44-100 Gliwice, Poland
[2]AGH University of Science and Technology, al. Mickiewicza 30, 30-059 Kraków, Poland
**Corresponding author: kperzyns@agh.edu.pl*

Abstract

Physical simulations were performed to identify and validate material models, which are used in optimization of manufacturing chains of fasteners. The focus was on hot rolling and controlled cooling. Physical simulations of thermo-mechanical processes were performed to validate microstructure evolution model for hot forming. Multi-stage deformations in the plane strain compression test were performed on the Gleeble 3800 simulator. Dilatometric tests were performed to identify and validate phase transformation model. Microstructure was investigated after each test using optical and electron microscopy. Good predictive capability of the models was confirmed.

Key words: material models, validation, bainitic steels, hot rolling, controlled cooling

1. INTRODUCTION

Numerous examples of optimization of technological parameters for a single forming process can be found in the scientific literature (Kusiak & Thompson, 1989). Considering not only one particular manufacturing process, i.e. forging, but modelling of the entire production chain is now an objective of research in many laboratories. It is expected that this approach would provide possibility of accounting for relations between subsequent operations (Hon & Xu, 2007; Pereira & Paulre, 2001; Madej et al., 2008; Pietrzyk et al., 2008; Kuziak et al., 2011). An increase of the strength-to-mass ratio, improvement of the dimensional accuracy and product properties (strength, ductility, fatigue resistance etc.), as well as decreasing the production costs is the objective of this optimization. Quality of the optimization depends on two aspects. The first is accuracy of the material models, which determine reliability and practical usefulness of the obtained results. Efficiency of the optimization procedure, which is determined by the computing times, is the second aspect. The first is the objective of the present work.

Two material problems are considered in the paper. The first is an application of the physical simulation to validate material models used in numerical modelling of manufacturing chains. The second is searching for new materials, which will allow to improve properties of product. This second objective was stimulated by promising results obtained by Kuziak et al. (2011) for manufacturing of fasteners made of bainitic steels. The preliminary research described by Waengler et al. (2008) and Kuziak et al. (2011) have shown that the new generation bainitic steels have some favourable features. These steels are characterized by high strength properties and reasonably good ductility (Bhadeshia & Edmonds, 1980), what creates wide possibilities of

ISSN 1641-8581

their applications. Manufacturing of high strength fasteners without heat treatment became possible. These steels were used in the present study for validation of material models. The paper is a continuation of (Kuziak et al., 2011). Additional micrographs are included in the analysis, including EBSD, and validation of the models is added.

2. NEW GENERATION BAINITIC STEELS FOR FASTENERS

More information on classification and morphological types of bainite particularly suitable for manufacturing of fasteners can be found in (Kuziak et al., 2011). Summary of this information is given below. Classical bainite is defined as micro-composite composed of bainitic ferrite and carbides, resulting from the austenite decomposition, which precipitate in a non-coordinated way together with the ferrite. Bainitic transformation combines features of diffusive and non-diffusive (controlled by slip) transformations (Bhadeshia & Edmonds, 1980). Lack of coordination causes that in the initial stage of the transformation, bainitic ferrite is formed and, after that, the carbon enrichment of the remaining austenite starts, eventually followed by the formation of carbides. However, by proper design of the bainitic steels chemical composition, the decomposition of austenite may be suppressed, and as a result blocky austenite or in the form of thin layers surrounded by bainitic ferrite plates is maintained in the final microstructure.

It has been shown in a number of publications that a granular bainite, which occurs in the high temperature range of the bainitic transformation, combines high strength with good ductility. It is due to a steep gradient of the carbon concentration in the remaining austenite and, in consequence, to the differentiation of the products of subsequent transformations in its volume. High carbon concentration close to the interface causes stabilization of the austenite in this area. The centre the austenite with lower carbon concentration is transformed into phases characterised by high ductility, which can be further increased by a decrease of the size of the hard particles in the granular bainite. It is shown by Kuziak et al. (2011) that the morphology presented in figure 1a, characterized by small and uniformly distributed martensite-austenite (MA) particles in the bainitic ferrite matrix, is the most suitable for cold forming. In the morphology shown in figure 1b the second phase has complex structure composed of outer layer of the retained austenite and products of incomplete austenite decomposition located in the centre.

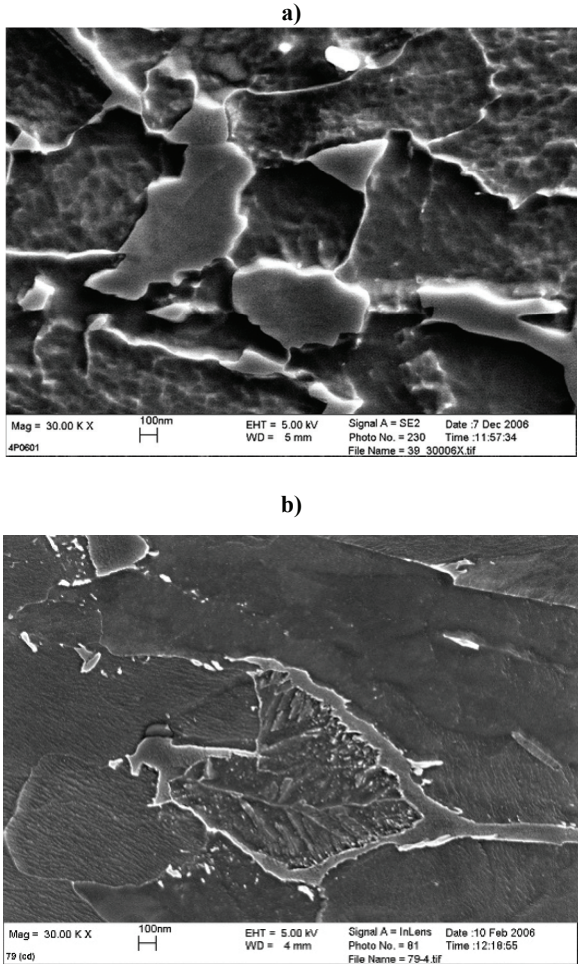

Fig. 1. *Microstructure of the granular bainite in the NiTiB steel, in which MA particles are the hard components (a) and granular bainite in the CrNiV steel, in which the second phase has complex structure composed of outer layer of the retained austenite and products of the incomplete austenite decomposition in the centre (b); FEM-SEM (Kuziak et al., 2011).*

3. EXPERIMENTS

The objective of the experiments was an investigation of the influence of processing parameters on morphology and mechanical properties of bainitic steels. Determined relationships were used to validate material models used in the optimization.

3.1. Materials

Several bainitic steels with various chemical compositions have been tested and their chemical compositions are given in table 1. The main idea of designing the compositions of experimental steels was to develop the granular bainite morphology in wire rod cooled in the Stelmor line and to strengthen the bainitic ferrite matrix with titanium carbide, TiC, particles. Steel 1210 has been selected for presentation of the results and all the models in this work were validated for the selected steel.

Table 1. *Chemical composition (wt %) of the investigated steels.*

steel	C	Mn	Si	Al	Cu	Nb	Ti	P	S	B	N
1210	0.074	2.0	0.28	0.034	0.10	0.038	0.13	0.012	0.011	0.002	0.0038
1211	0.072	1.88	0.24	0.034	0.11	0.062	0.13	0.012	0.011	0.002	0.0038
1212	0.067	1.93	0.26	0.026	0.11	0.033	0.13	0.012	0.011	0.002	0.0036
1213	0.073	1.89	0.27	0.028	0.20	0.033	0.13	0.010	0.010	0.002	0.0036
1214	0.060	1.92	0.27	0.025	0.22	0.031	0.13	0.013	0.013	0.002	0.0035

3.2. Thermophysical modelling of rolling

The objective of this experiments was supplying data for the validation of the microstructure evolution model. Detailed description of these experiments is given by Kuziak et al. (2011). Briefly, the multistage plane strain compression tests were performed on the simulator Gleeble 3800 with the following procedures: samples with dimensions 10 mm in diameter and 12 mm in height were preheated to 1200°C, maintained at that temperature for 60 s and deformed in four passes at 1100°C, 1050°C, 980°C or 800°C. Parameters of multistage deformation are given in table 2. Deformation in all stages was 0.3. Cooling after the last deformation was composed of two stages. Fast cooling (10°C/s) to the temperatures T_{fc} = 400°C-550°C that was supposed to simulate cooling in the Stelmor line was first. Slow cooling with the rate of 0.2°C/s, which simulated free air cooling of the coil, was applied next. Cooling variants are given in table 3.

Mechanical properties of samples were measured after each test and the results are given in table 4. Due to the small size of the sample used in the multi-stage deformation experiment, the small (non-standardized) sample was machined for the tensile test. As a result, the values of the measured elongation and reduction in area are to be interpreted only for the sake of the comparison of different cooling patterns. On the contrary, proof strength and ultimate tensile strength are measured with the reasonable accuracy. Selected microstructures for the last deformation temperature of 980°C are shown in figures 2-5. Similar microstructures for the last deformation temperature of 800°C are shown in figures 6-8. The etching with 2% Nital solution revealed prior austenite grain boundaries (figure 2). Analysis of results of thermomechanical simulations shows that last deformation temperature T_{fr} = 980°C yields recrystallized microstructure and grain size in a range of 25-30 μm. The microstructures developed inside the grains differ according to the temperature at which the fast cooling at a rate of 10°C was stopped.

Table 2. *Variants of thermomechanical simulations.*

Variant	T, °C	$\dot{\varepsilon}$, s^{-1}	t, s	T, °C	$\dot{\varepsilon}$, s^{-1}	t, s	T, °C	$\dot{\varepsilon}$, s^{-1}
1 2	1100	1	25	1050	2	14 50	980 800	10(a), 20(b), 50(c)

Table 3. *Variants of thermomechanical simulations.*

Variant	044Temperature/cooling rate		
1	980 → 550 / 10	550 → 200 / 0.2	200 → RT
2	800 → 550 / 10	550 → 200 / 0.2	200 → RT
3	980 → 500 / 10	500 → 200 / 0.2	200 → RT
4	800 → 500 / 10	500 → 200 / 0.2	200 → RT
5	980 → 450 / 10	450 → 200 / 0.2	200 → RT
6	800 → 450 / 10	450 → 200 / 0.2	200 → RT
7	980 → 400 / 10	400 → 200 / 0.2	200 → RT
8	800 → 400 / 10	400 → 200 / 0.2	200 → RT

Table 4. *Mechanical properties after various variants of thermomechanical simulations.*

Variant	$Rp_{0.2}$, MPa	R_m, MPa	$A_{1.5}$, %	Z, %
1	669	782	39	67
3	751	847	41	73
5	639	692	37	83
7	849	947	42	73
2	634	882	44	69
4	597	783	42	65
6	687	782	47	73
8	711	792	38	73

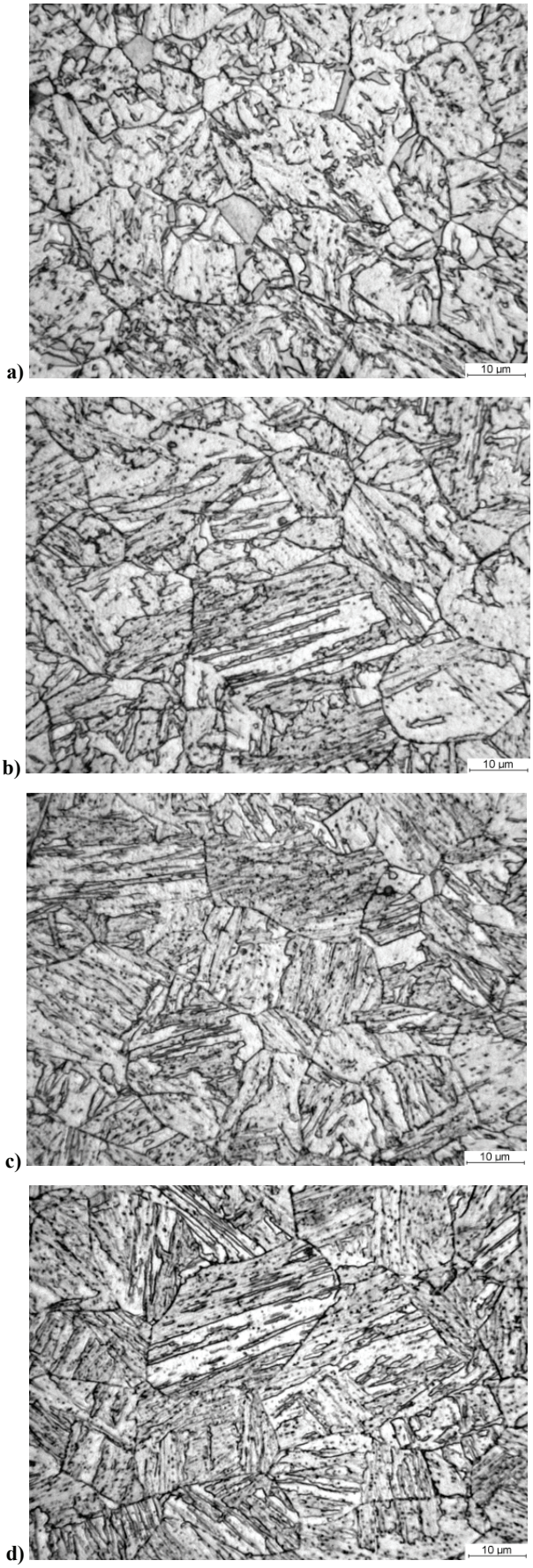

Fig. 2. Microstructures of the steel 1210 after physical simulation of hot rolling with the last deformation at 980°C; variant 1 (a); variant 3 (b); variant 5 (c); variant 7 (d) (Kuziak et al., 2011). Optical microscope.

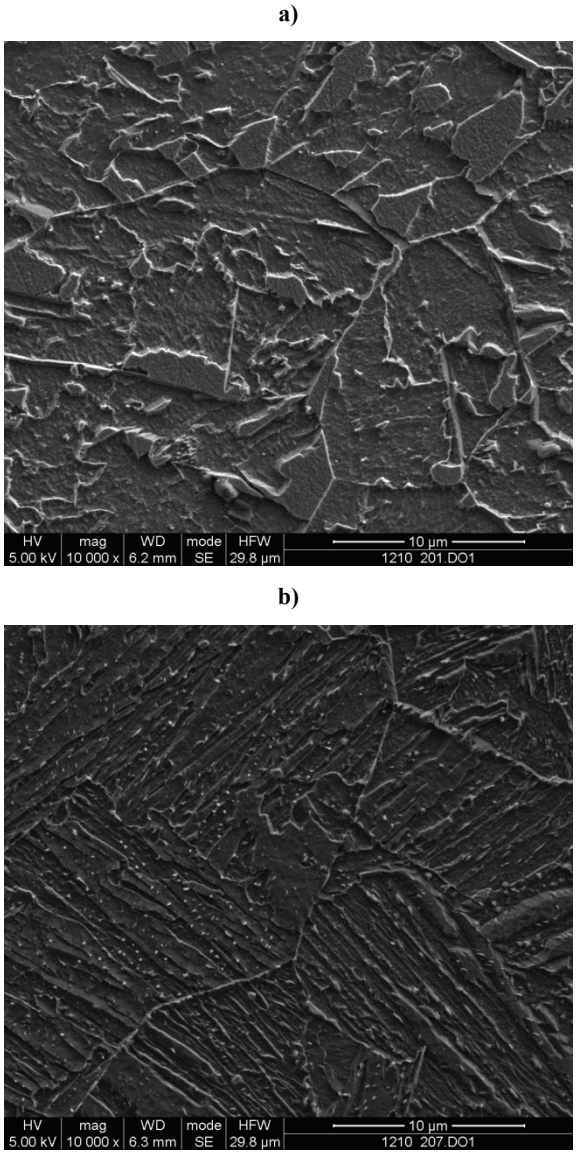

Fig. 3. Microstructures of the steel 1210 after physical simulation of hot rolling with the last deformation at 980°C; variant 1 (a); variant 7 (b). FEG SEM. (Kuziak et al., 2011).

Accelerated cooling to the temperature 550°C gives microstructure of the granular bainite, but the "hard" constituent particles are large and located at the austenite grain boundaries. The latter may decrease the ductility (table 4). Decrease of the temperature of the end of the accelerated cooling to 500-450°C causes a decrease in the amount of the granular bainite while volume fraction of the lower and upper bainite increases. When fast cooling ends at 400°C tempered martensite occurs in the microstructure. In general, decrease of the temperature of the end of the accelerated cooling gives an increase in strength without a decrease in the ductility.

As seen in figure 3a the hard constituent of granular bainite is non-uniformly distributed and contains tempered martensite, retained austenite and

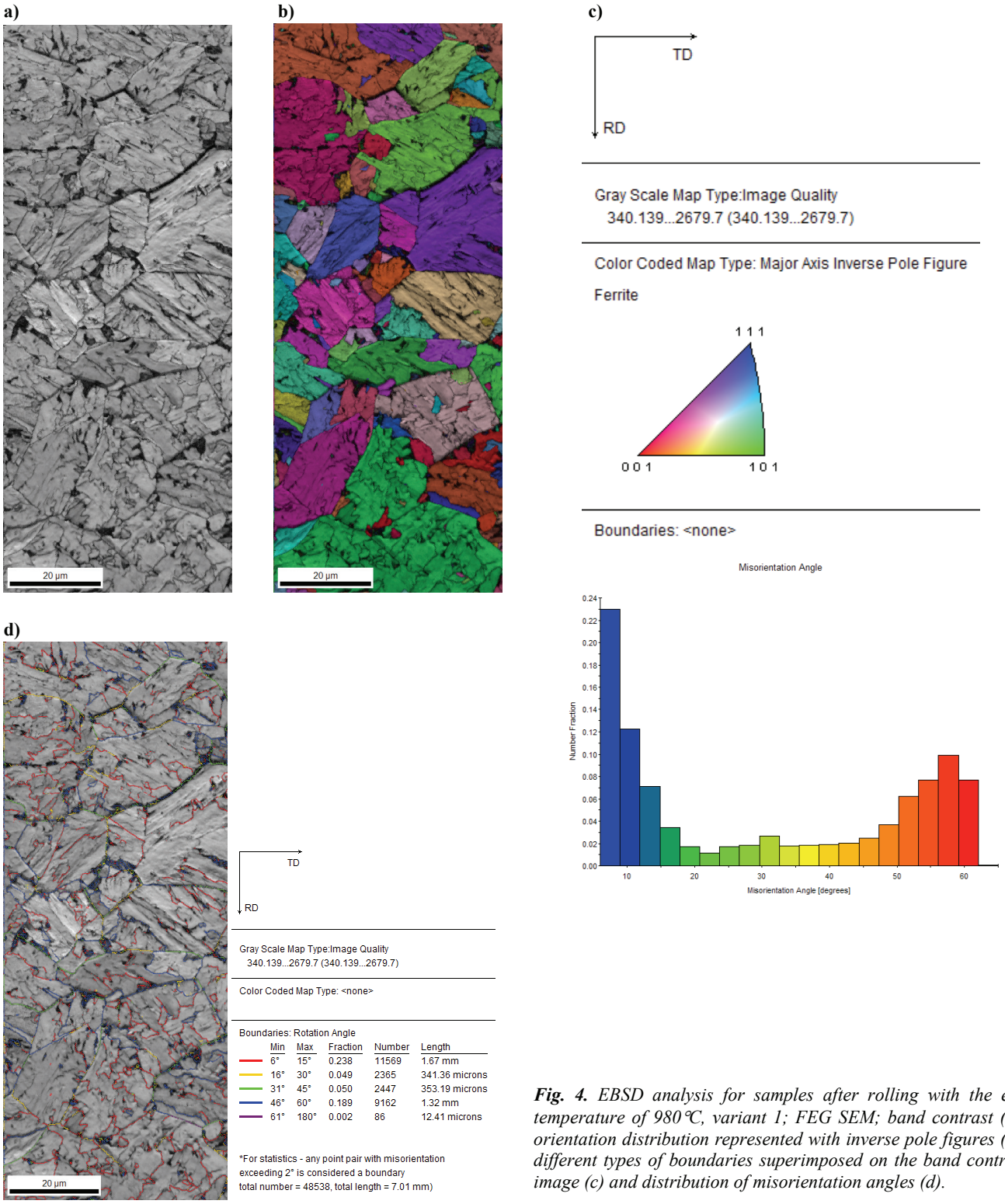

Fig. 4. *EBSD analysis for samples after rolling with the end temperature of 980 ℃, variant 1; FEG SEM; band contrast (a); orientation distribution represented with inverse pole figures (b); different types of boundaries superimposed on the band contrast image (c) and distribution of misorientation angles (d).*

high carbon bainite or a mixture of ferrite and cementite. Analysis of microstructures combined with the data in table 4 confirms that increase in strength and ductility is due to the dispersion of the hard constituent particles. Changes of mechanical properties may also be due to variations of the bainite grain size caused by changes of the end temperature of the accelerated cooling. This correlation was investigated using EBSD technique (figure 4). In spite of occurrence of the substructure, after bainitic transformation, in general one crystallographic orientation was formed in the bainitic ferrite within the austenite grains. In consequence, an effective grain size of the bainitic ferrite is comparable with the size of the former austenite grains. This microstructure caused decrease of ductility in temperatures below 0°C. Decrease of the end temperature of the accelerated cooling involves change of the morphology of the bainitic ferrite from the granular to lamellar. Lamellas within one grain have different orientations.

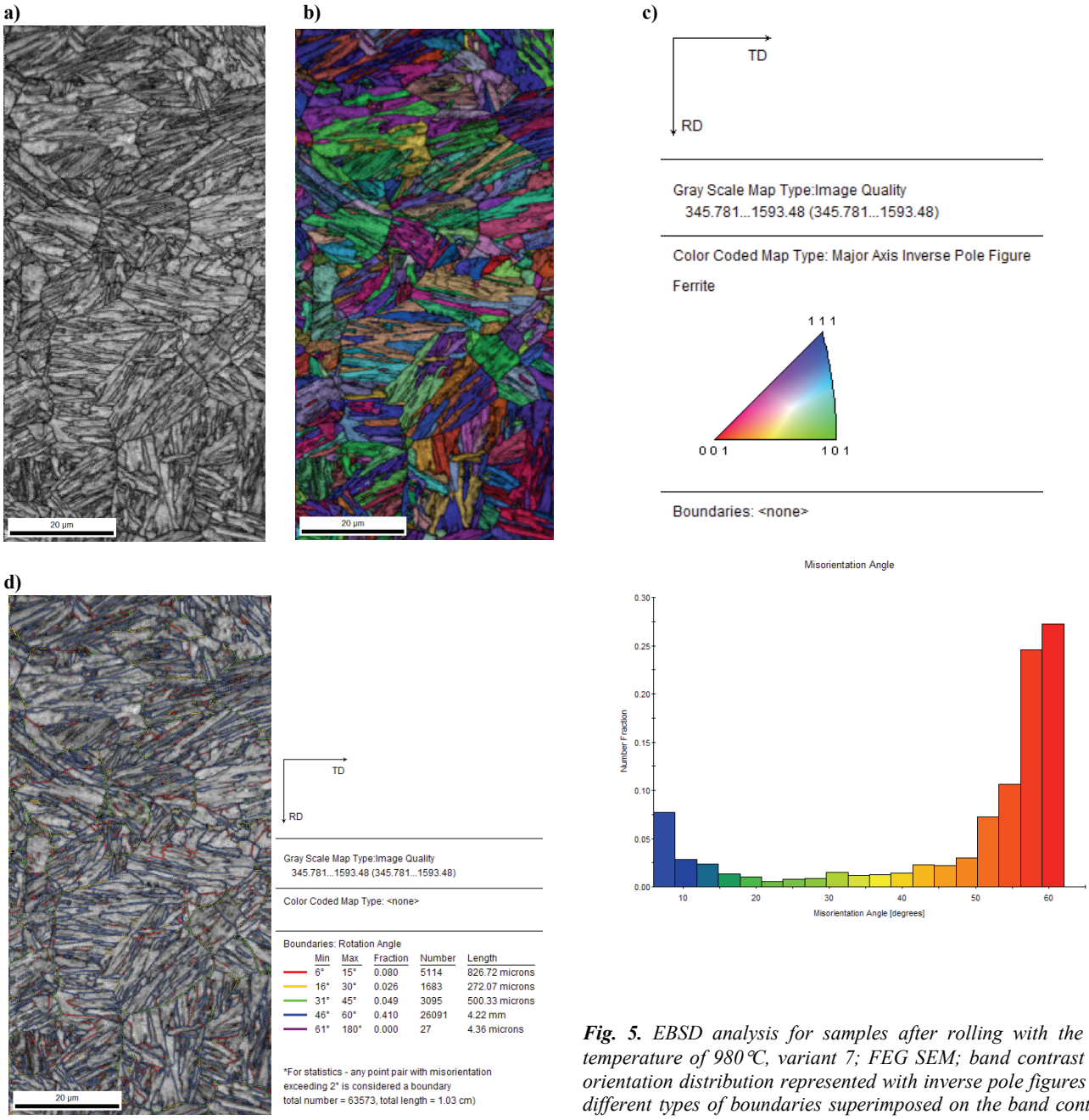

Fig. 5. *EBSD analysis for samples after rolling with the end temperature of 980°C, variant 7; FEG SEM; band contrast (a); orientation distribution represented with inverse pole figures (b); different types of boundaries superimposed on the band contrast image (c) and distribution of misorientation angles (e).*

The granular bainite morphology is shown in figure 4. This morphology was developed by stopping the fast cooling at 550°C, what gave relatively high temperature of the bainitic transformation. The irregular ferrite grains in this case, which are the constituent of granular bainite, are encompassed by prior austenite grains and typically one crystallographic orientation is developed in one austenite grain (figure 4b). Therefore, the boundaries inside the grains in figure 4c are essentially low-angle boundaries and their distribution is in the range of 0-15° (figure 4e). The distribution of the boundaries in the range of 15-45° corresponds to the misorientation between grains formed in the different austenite grains. The peak around 55-60° originates from grains formed within one austenite grain but with different orientation relationship. In bainitic steels, the crystal orientations typically lie within the Bain region, which is encompassed by Kurdjumov-Sachs and Nishiyama-Wassermann relationships.

Different EBSD pattern was obtained after fast cooling to 400°C (figure 5). In this case, lath like morphology of bainite was developed within the austenite grains. Several laths having the same crystallographic orientation are grouped in distinct units called packets. Up to 6 such packets could be formed in one grain, which resulted in an increase in the number of grain boundaries with misorientation angle in the range of 55-60°. Despite, the highest

strengths, such a microstructure is also characterized by high ductility.

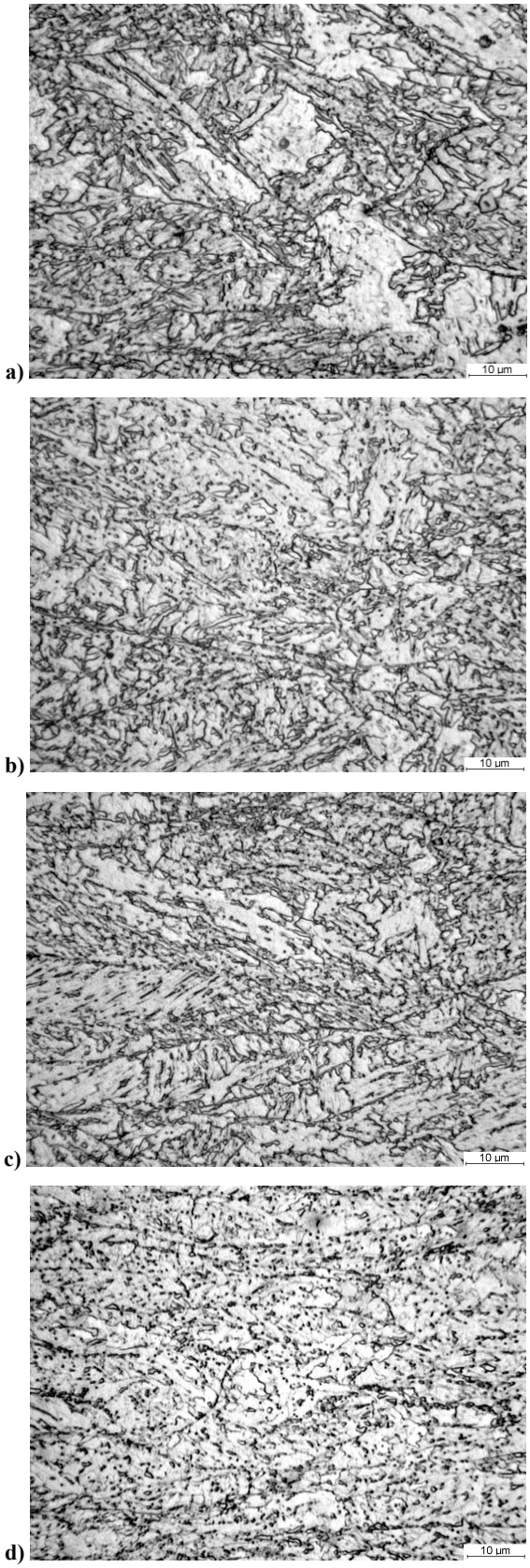

Fig. 6. *Microstructures of the steel 1210 after physical simulation of hot rolling with the last deformation at 800°C; variant 2 (a) (Kuziak et al., 2011); variant 4 (b); variant 6 (c); variant 8 (d) (Kuziak et al., 2011). Optical microscope.*

Analysis of microstructures of samples with the temperature of the last deformation 800°C (figures 6, 7 and 8) shows larger contribution of the alotrimorphic ferrite. Beyond this, the main difference is concerned with the type of the bainitic microstructure, which is composed mainly of bainitic ferrite. This is due to an increase of the nucleation sites and an increase of the diffusion rate caused by the dislocation substructure since the deformation temperature of 800° lies below recrystallization stop temperature. Strength of these samples is lower that those with the T_{fr} = 980°C, what is due to larger volume fraction of the ferrite. Transformation from the non recrystallized austenite gives more uniform microstructure.

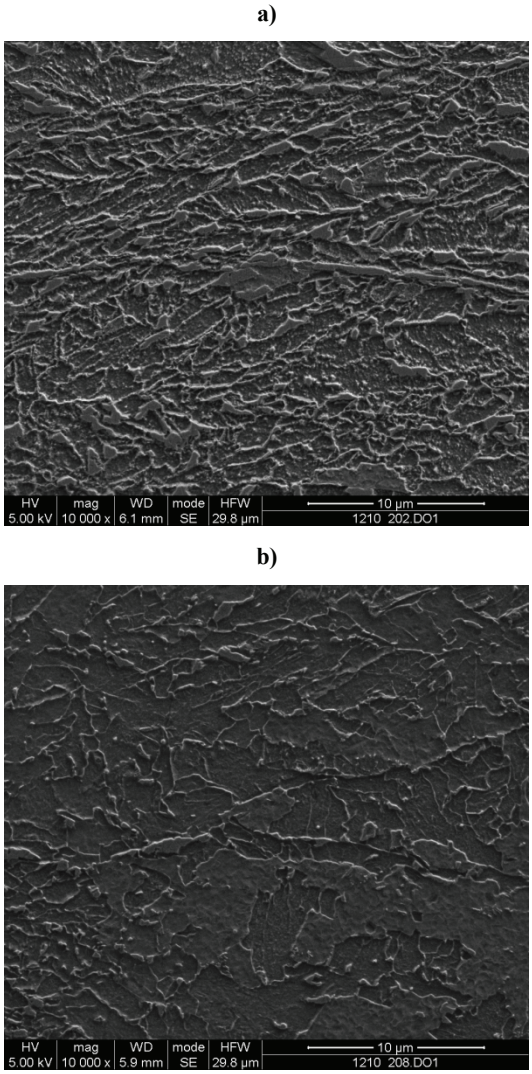

Fig. 7. *Microstructures of the steel 1210 after physical simulation of hot rolling with the last deformation at 800°C; variant 1 (a); variant 8 (b). FEG SEM. (Kuziak et al., 2011).*

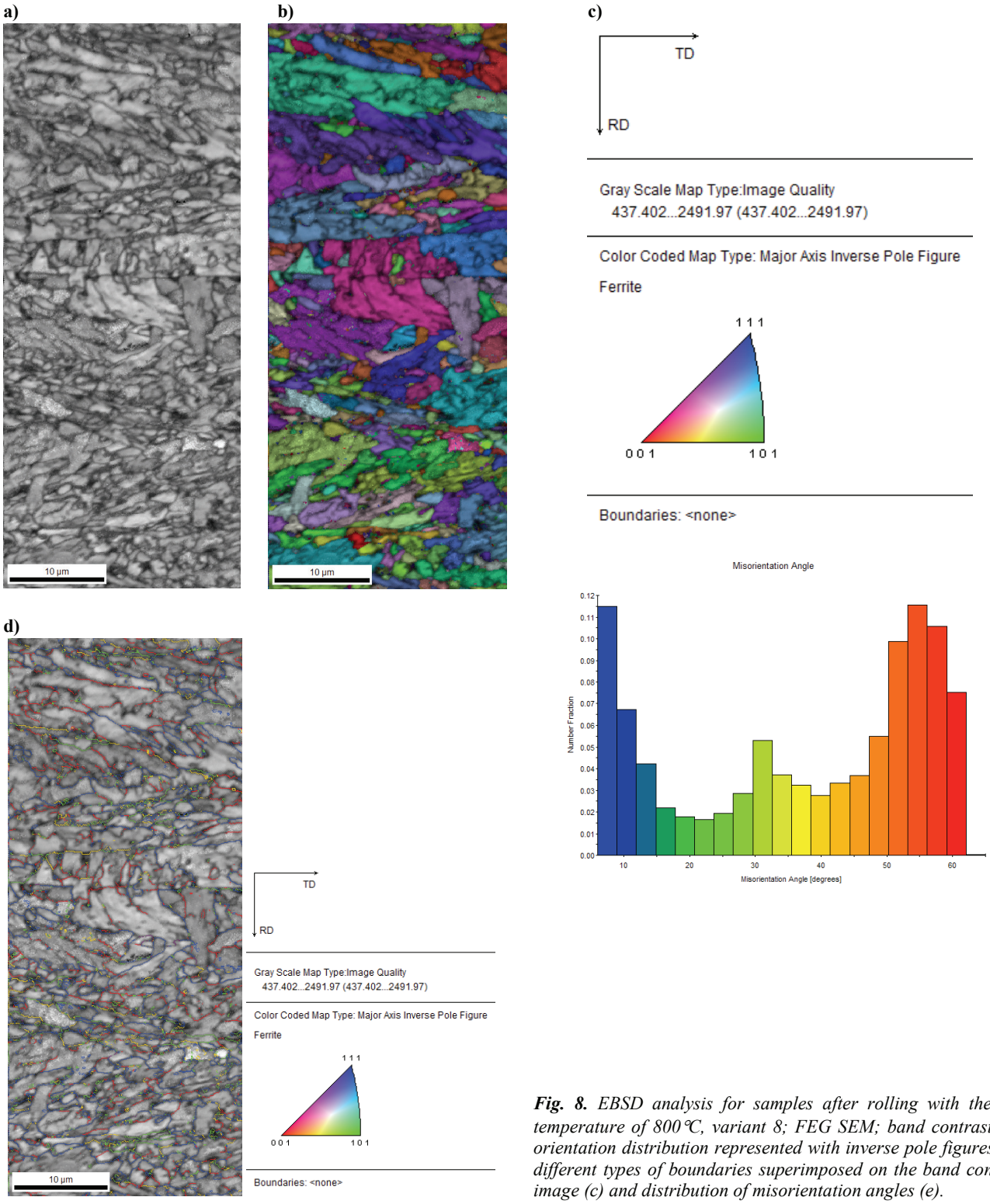

Fig. 8. *EBSD analysis for samples after rolling with the end temperature of 800°C, variant 8; FEG SEM; band contrast (a); orientation distribution represented with inverse pole figures (b); different types of boundaries superimposed on the band contrast image (c) and distribution of misorientation angles (e).*

Analysis of the EBSD (figure 8) shows that the effective grain size in these samples decreases comparing to that obtained from the recrystallized austenite. This is associated with the fact that the deformation bands act as effective nucleation sites. Figure 8 clearly show that the number of boundaries with the peak around 55-60° increased comparing to the microstructure shown in figure 4.

One of the most important problem connected with the bainitic microstructures is the definition of so-called effective grain size. In this research, it was assumed that the bainitic grain is defined as the size of the microstructural unit separated from the neighboring grains by an angle greater than 15°. From the EBSD results, it is evident that in the case of granular bainite, the effective grain is equal to one or a group of irregular ferrite "grains" seen in the opti-

cal microscopy images. In the case of lath-like bainites, the effective grain is composed of several bainitic ferrite grains.

The effect of the processing conditions on the distribution of effective grain is seen in figure 9.

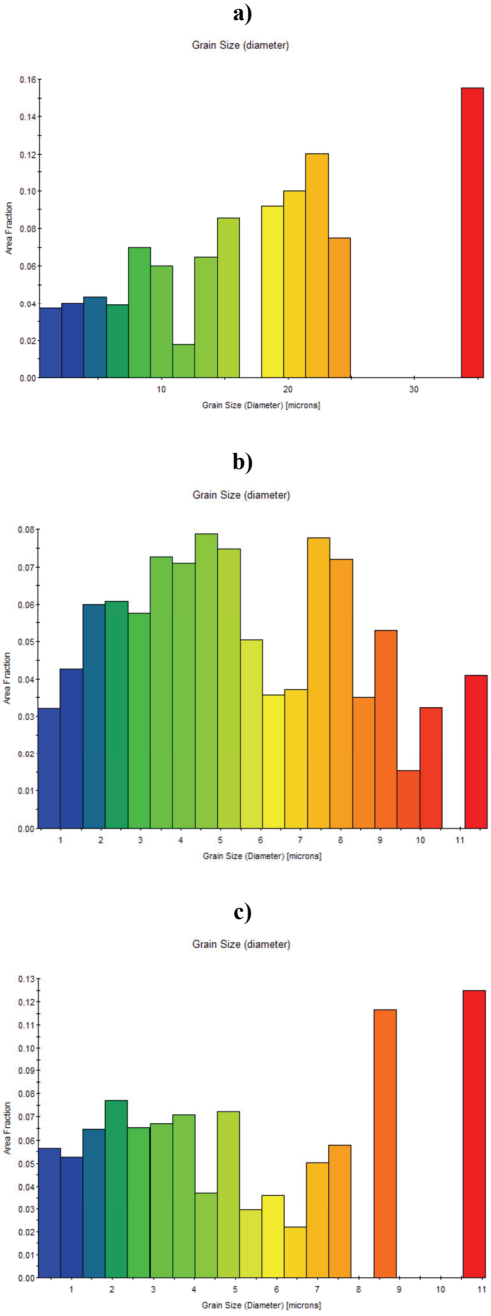

Fig. 9. *Grain size distribution measured using EBSD technique: after variant 1 (a); after variant 7 (b); after variant (8) (c).*

It can be seen that the size of the grains in the sample subject to variant 1 is comparable with the austenite grain size. This is attributed to the fact that one or at maximum three different orientation variants are developed in one austenite grain during the transformation. Grain sizes in the sample subject to variant 7 and 8 are comparable, but, from different reasons. The meaning of the grain size in the case of lath-like microstructures (variant 7) is connected with the individual packet size. This is an effect of lowering the bainitic transformation temperature. In the case of the sample subject to variant 8, the effective grain can be connected to the group of irregular ferrite subgrains, and results from the deformation below the recrystallization stop temperature.

3.3. Rod rolling in the pilot mill

The rolling process for bainitic steel rods was conducted on the three–high laboratory rolling mill. The details of the experiment performed in this project are given by Kuziak et al. (2011). Briefly, the square bars 49×49 mm were subject to the pre–rolling in 3 oval-round-square passes to the square 23×23 mm, followed by 4 oval-round passes during the finish rolling to the bar having diameter of 15.8 mm. The finish rolling temperature was varied by changing the holding time prior to the first pass. After rolling, the bars were subject to the accelerated cooling with pressurized air. The cooling rates at the cooling device were varied by applying different air pressure. Figure 10 shows locations at the bar cross section where the measurement of the austenite grain size was conducted. Results of measurements are given in table 5.

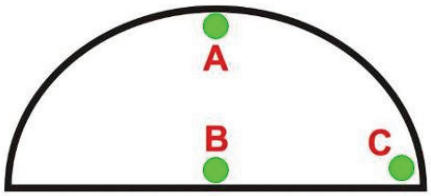

Fig. 10. *Locations at the bar cross section where the measurement of the austenite grain size was conducted.*

Table 5. *Results of the austenite grain size measurements in the areas A, B, C of the bars.*

T_{fr}, °C	Grain size, μm		
	A	B	C
1050	39.7	32.5	35.5
950	28.3	27.3	29.8

3.4. Dilatometric tests

The objective of these experiments was supplying more accurate and reliable data for the phase transformation models and an investigation of the influence of plastic deformation and controlled cooling on morphology and mechanical properties of

bainitic steels. The tests were performed on the dilatometer DIL 805 with the following procedures:

1. Austenitization temperature and time: 1200°C/60s; deformation temperature and strain: 1000°C/0.6; cooling rate 0.5-67°C/s.
2. Austenitization temperature and time: 1200°C/60s; deformation temperature and strain: 870°C/0.6; cooling rate 0.5-67°C/s.

When deformation was at 1000°C austenite was fully recrystallized at the beginning of the transformation. When deformation was at 870°C recrystallization was not completed before the transformation. Comparison of the CCT diagram for the recrystallized and not recrystallized austenite for steel 1210 is shown in figure 11. Microstructures for different cooling rates are shown in figure 12. It is seen that deformation of the austenite accelerates the ferritic transformation and decreases the start temperature of the bainitic transformation. In consequence the volume fraction of the ferrite increases and microstructures composed of alotrimorphic and bainitic ferrite are favourable. Austenite is richer in carbon and can transform into high-carbon bainite and martensitic-austenitic (MA) islands. The effect of the austenite deformation on the pearlitic and martensitic transformations is small. Similar results were obtained for the remaining steels. Pearlite should be avoided to improve ductility of bainitic steels and cooling rates should exceed 2-3°C/s.

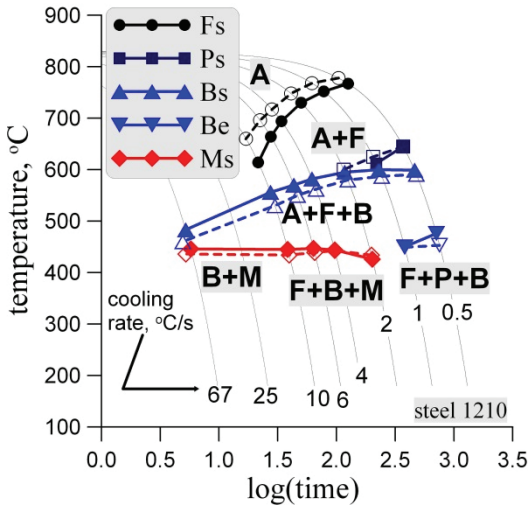

Fig. 11. CCT diagram for the recrystallized austenite (deformation at 1000°C - full symbols and solid lines) compared with non-recrystallized austenite (deformation at 870°C - open symbols and dotted lines).

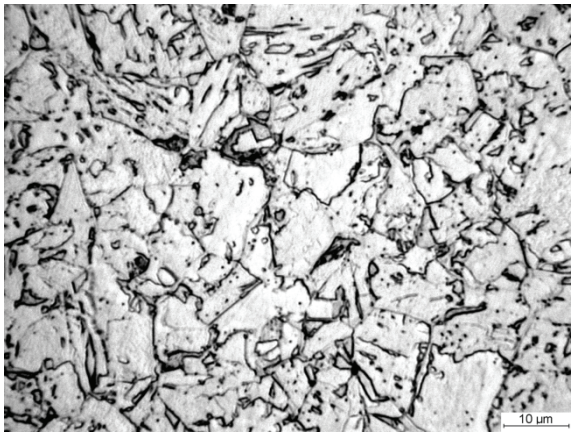

1°C/s (F+B+P)

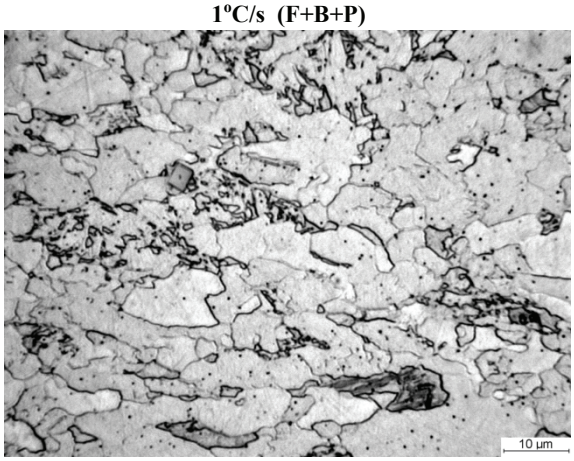

1°C/s (F + B + P)

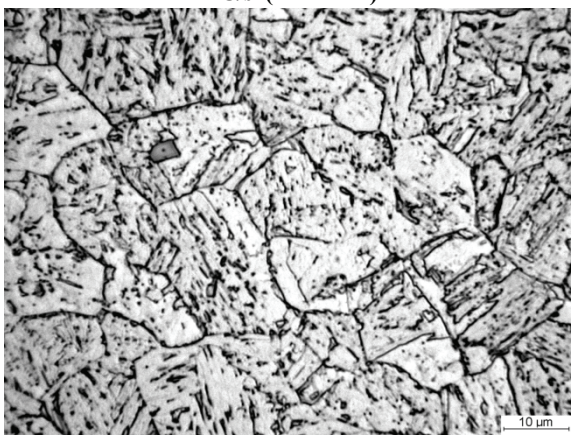

4°C/s (B +F + M)

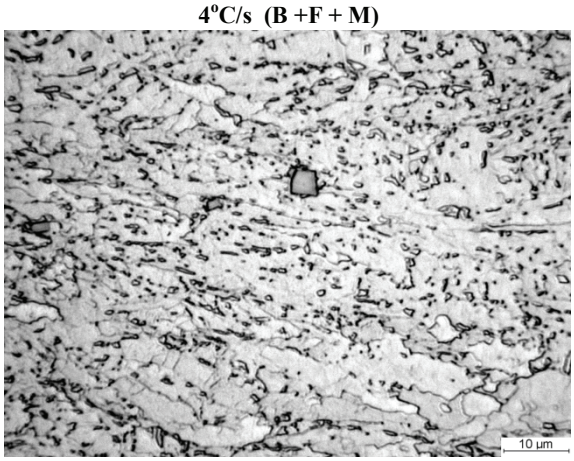

4°C/s (F + B + M)

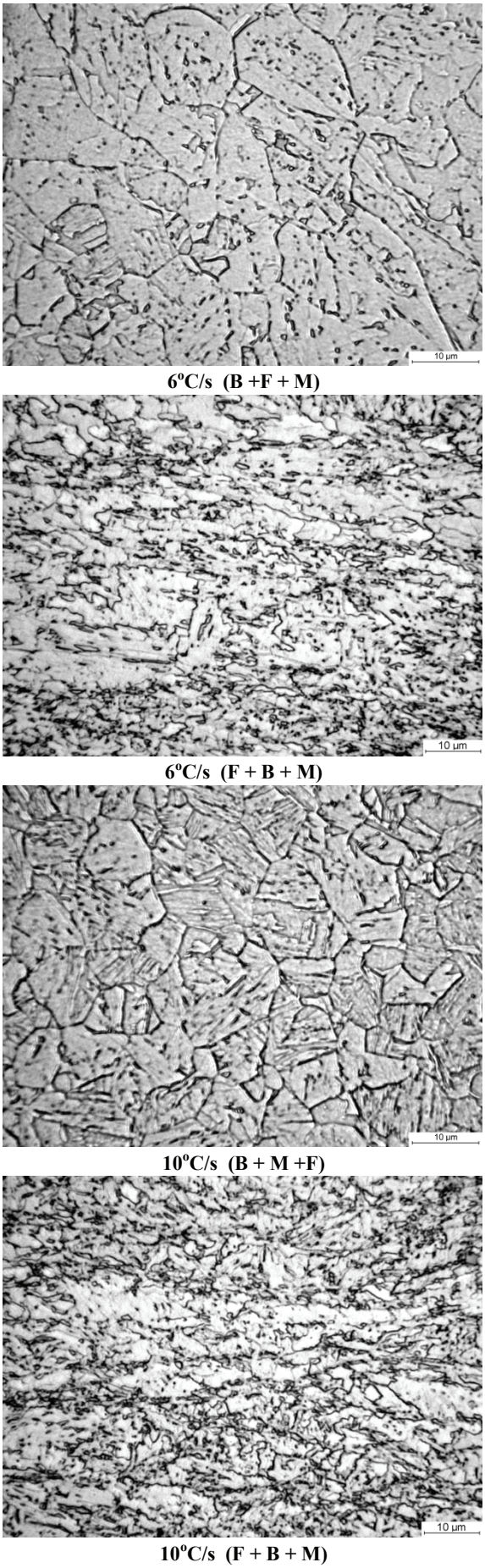

Fig. 12. Microstructures after deformation at 1000°C (left) and 870°C (right) and various cooling rates.

Optimal microstructure of granular bainite is obtained for the transformation of non-recrystallized austenite, which gives high dispersion of the second phase particles. Having this in mind the optimal cooling rate was proposed in the range of 4-10°C/s.

3.5. Summary of experiments

Recapitulating the analysis of the experimental data allowed following conclusions:

- Deformation below the recrystallization temperature promotes the occurrence of the granular bainite, see figure 12 (right).
- In non recrystallized austenite ferrite occurs at higher cooling rates comparing to the recrystallized austenite.
- For low cooling rates (C_r < 2°C/s) granular bainite is characterized by relatively large grain size and large dimension of the hard component, which is non uniformly distributed in the steel structure. It means that cooling rate after hot rolling should be in the range of 3-6°C/s. This cooling rate can be easily reached in the Stelmor system.
- Accelerated cooling should be finished at the temperature of 400-450°C.

Objectives for the optimization of the manufacturing chain were formulated having above conclusions in mind.

4. MODELS

Simulations were performed using commercial Abaqus finite element (FE) software. Rheological and microstructure evolution models developed for the bainitic steels were implemented in the FE code via the UHARD subroutine and are briefly described below.

4.1. FE model

Conventional isotropic elasto-plastic flow rule was used during the calculations. This model can be explained as an expansion of the yield surface without any change in the position of its centre. The approach is commonly used for modelling metal plasticity, either as a rate-dependent or as a rate-independent model. Due to the fact that, elastic and plastic behaviour is considered the decomposition of strains into elastic and plastic parts is described as:

$$\varepsilon = \varepsilon^e + \varepsilon^p \qquad (1)$$

incompressibility condition takes the form:

$$I : \varepsilon^e = \varepsilon_{11}^p + \varepsilon_{22}^p + \varepsilon_{33}^p = 0 \tag{2}$$

where: I - second order identity tensor.

The von Mises yield criterion is used during simulation ($f < 0$ when elastic deformation, $f = 0$ when plastic deformation):

$$f = \sigma_e - \sigma_Y = \sqrt{\frac{3}{2}\sigma^I : \sigma^I} - \sigma_Y \tag{3}$$

where: σ_e - effective stress, σ_Y - yield stress, σ^I - deviatoric stress tensor.

The flow theory is described as:

$$d\varepsilon^p = d\lambda \frac{\partial f}{\partial \sigma} \tag{4}$$

where: df – the plastic potential:

$$df = \frac{\partial f}{\partial \sigma} d\sigma + \frac{\partial f}{\partial \varepsilon_p} d\varepsilon_p = 0 \tag{5}$$

In the case of von Mises model:

$$d\lambda = d\varepsilon_p = \sqrt{\frac{2}{3} d\varepsilon^p : d\varepsilon^p} \tag{6}$$

Presented mechanical model is additionally coupled with the finite element solution of the Fourier heat transport equation:

$$\nabla \cdot k \nabla T + Q = \rho c_p \frac{\partial T}{\partial t} \tag{7}$$

where: k – heat conductivity, T – temperature, Q – rate of heat generation due to plastic work or due to transformation, ρ – density, c_p – specific heat, t – time.

4.2. Rheological model

Rheological model for hot forming was developed and incorporated into the Abaqus software via UHARD subroutine. Coefficients in these models were determined using plastometric tests performed on the Gleeble 3800 simulator. The stress-strain curves obtained in the uniaxial compressing tests were processed by means of the inverse technique to eliminate the effect of friction and adiabatic heating. The inverse algorithm described by Szeliga et al. (2006) was used. It was found by Kuziak et al. (2011) that the rheological model developed at the University of Sheffield (Davenport et al., 1999) and described also by Kowalski et al. (2000), was successfully fitted with the experimental stress-strain curves for wide range of hot forming temperatures. This model contains 16 coefficients and creates problems with identification. Since the present work is focused on finishing passes characterized by low values of the Zener-Hollomon parameter, the effect of the dynamic recrystallization can be neglected and simple equation proposed by Hansel & Spittel (1979) was used:

$$\sigma_p = A\varepsilon^m \exp(q\varepsilon)\dot{\varepsilon}^n \exp(\beta T) \tag{8}$$

where: T – temperature in ^{o}C, A, m, n, q, β - coefficients, which were determined using the inverse method (Szeliga et al., 2006). Values of these coefficients obtained from the inverse analysis are given in table 6. The final value of the cost function Φ, which is the square root error between measured and calculated forces and which represents accuracy of the inverse analysis, is given in the last column of this table 6. Selected flow stress curves are shown in figure 13.

Table 6. *Coefficients in equation (8) for the steel 1210 obtained from the inverse analysis.*

A	m	q	n	β	Φ
1089.7	0.072	0.107	0.00464	0.0826	0.0299

4.3. Microstructure evolution model

Development of the microstructure evolution model for the experimental bainitic steels, capable of predicting changes in the austenite microstructure occurring in the rod or wire rolling process, is described by Kuziak et al. (2011). The model equations allow the prediction of the following parameters and phenomena occurring in the deformed material:

- kinetics of the dynamic, metadynamic and static recrystallization,
- recrystallized grain size,
- kinetics of grain growth after recrystallization,
- static recovery.

A closed form equations are used to characterize the effect of initial austenite grain size, strain, strain rate, temperature and time on the microstructural evolution during and after deformation are given in (Kuziak et al., 2011) and are not repeated here. Coefficients in those equations were determined using inverse analysis of the stress relaxation tests. Basic principles of these tests are described by Karjalainen and Perttu (1999).

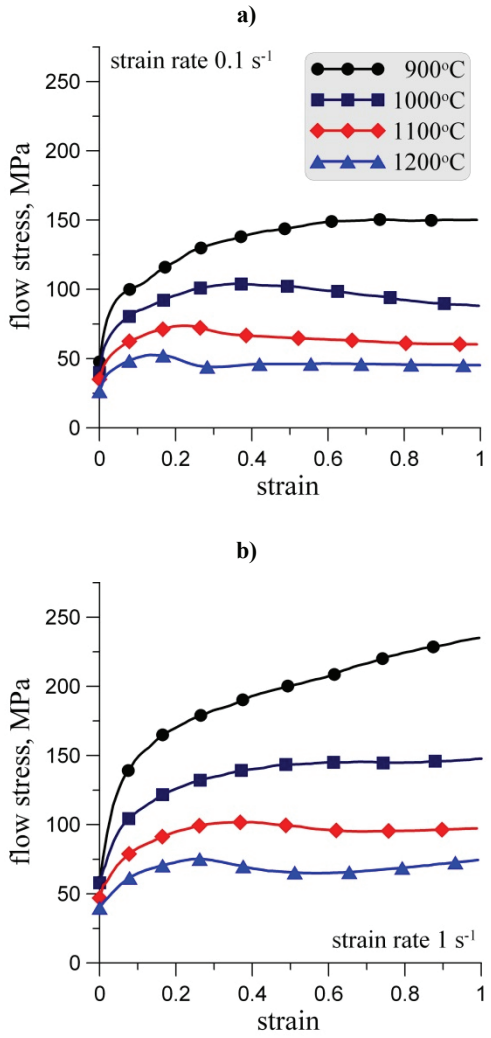

Fig. 13. Flow stress of the investigated bainitic steel obtained from the inverse analysis for the a) 0.1 and b) 1 s^{-1} strain rate and four different temperatures.

4.4. Phase transformation model

A simple model based on Avrami (1939) equation was selected in the present work:

$$X = 1 - \exp\left(-kt^n\right) \tag{9}$$

where: X – transformed volume fraction, k, n – coefficients.

Theoretical considerations show that, according to the type of transformation (nucleation and growth process, site saturation process) a constant value of coefficient n in equation (9) can be used. On contrary, value of the coefficient k must vary with temperature in a way linked to the form of a TTT diagram. The formalism of the function $k = f(T)$ must be carefully chosen to describe properly the temperature dependence of k. Function for the ferritic transformation, as well as models for the remaining transformations, are given in (Kuziak et al., 2011). Coefficients in the phase transformation model calculated using inverse analysis for the deformation temperature of 1050°C and 870°C are given in (Kuziak et al., 2011), as well.

Phase transformation model with the optimized coefficients was implemented in the FE code and used in simulations of the accelerated cooling after hot rolling.

5. VALIDATION OF THE MODELS

Flow stress model, microstructure evolution model and phase transformation model were validated by comparison predictions with the experimental data.

5.1. Simulation of the rod rolling process

Hot rolling of rods or wires is the first link in the manufacturing chain, which is considered. The objective of simulations is prediction of microstructure evolution after hot rolling. The models described in sections 4.1 (FE model), 4.2 (rheological model) and 4.3 (microstructure evolution model), were applied.

The important module of the numerical calculation deals with the austenite grain size prediction prior phase transformation modelling. The evolution model describes austenite grain size as a function of initial grain size, strain, strain rate, temperature and time (Kuziak et al., 2011). Developed nnumerical model of rod rolling process in 2D space is presented in figure 14. For simplicity only the finishing rolling pass was investigated.

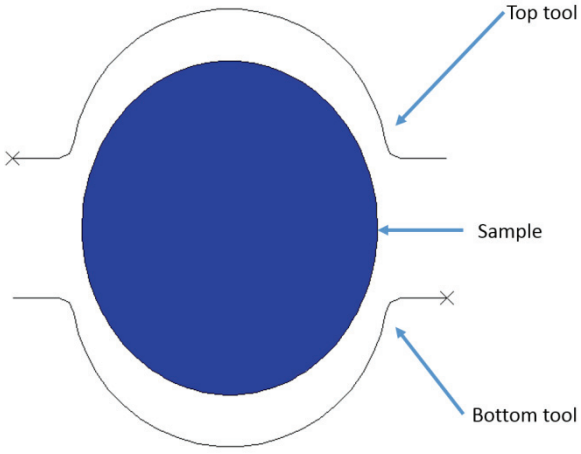

Fig. 14. Assembly of numerical model of last cage rolling rod process.

Upper and lower rolls are assumed to be non-deformable tools modeled as an analytical rigid material. The shape of the rod cross section is automatically generated by the Python script to provide pos-

sibility of investigation of influence of the initial shape on final results. Rolling is realized at the two different temperatures, 1050°C and 950°C, respectively. The following thermal parameters were selected: emissivity factor set to 0.8 and heat transfer coefficient between tools and sample set to 5000 W/m^{2}K. The microstructure evolution model assumes initial grain size equal to 30μm. Model was discretized with CPE4RT finite elements and an implicit thermal-displacement solver was applied to solve the investigated case study. Examples of obtained grain size distribution after rod rolling for the two investigated temperatures are shown in figure 15.

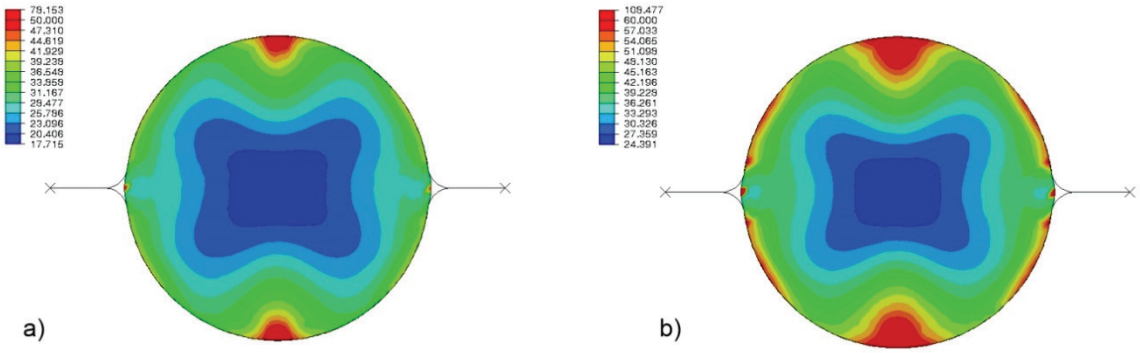

Fig. 15. *Grain size distribution after rod rolling at temperatures 950°C (a) and 1050°C (b).*

As seen the grain size distribution remains quite uniform across the sample. Significantly higher values were obtained only in the upper and lower regions of the rod, what is directly related with the shape of the rod prior finishing pass. In the future automatic optimization model developed in (Legwand et al., 2014) will be used to design initial shape of the sample that will provide uniform grain size distribution after finishing pass.

Results in figure 15 were validated by comparison with the measurements performed after experimental rod rolling. Three locations were selected for investigation, as shown in figure 10. Typical micrographs for the temperature of 950°C are shown in figure 16 while comparison between measured and calculated grain sizes is in figure 17.

As seen in figure 17, predicted and experimental grain sizes are in good agreement. Large differences are observed only in the top region (A) of the sample, where numerical model predicts larger values than the one observed experimentally. However, as it has been mentioned this behaviour can be eliminated by a proper design of the shape of the sample prior to finishing rolling.

5.2. Accelerated cooling

After hot rolling the rods and the wires were cooled using air under pressure. Cooling schedule described in section 2.2 was simulated. This schedule, which resembles the Stelmor system followed by cooling in the coil, is composed of fast cooling (10°C/s) to the temperatures T_{fc} = 400°C-550°C followed by slow cooling with the rate of 0.2°C/s. Results for T_{fc} = 550°C and 400°C are shown in figure 18.

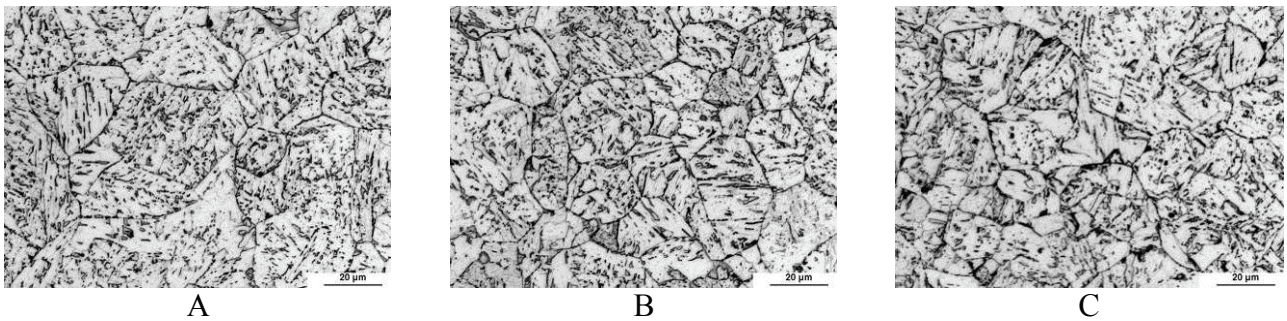

Fig. 16. *Microstructure at the locations A, B, C of the bar rolled with the last deformation temperature 950°C.*

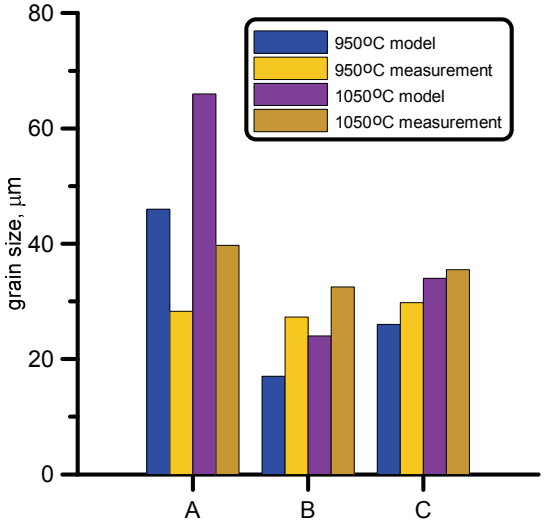

Fig. 17. Comparison between measured and calculated grain sizes in the investigated locations A, B and C for rolling temperatures 1050°C and 950°C.

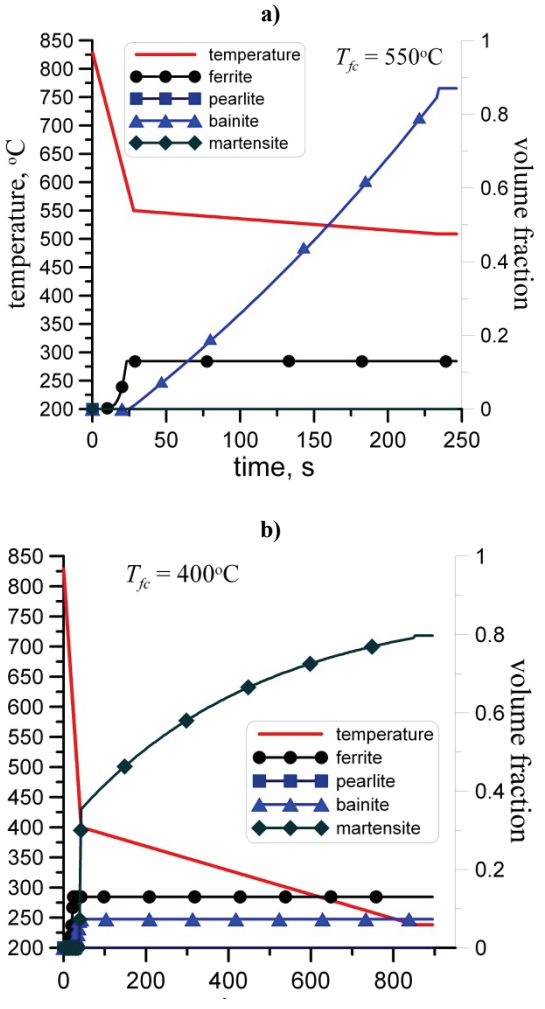

Fig. 18. Temperatures and kinetics of transformations during cooling from the last deformation temperature 980°C, end of fast cooling temperature 550°C (a) and 400°C (b).

6. CONCLUSIONS

Physical simulations of thermomechanical simulation were used to identify and verify the material models for bainitic steels. Compression tests were used to identify flow stress model and dilatometric tests were used to identify phase transformation model. The following conclusions were drawn:

- Physical simulations have shown that there is a wide possibility of influence on the microstructure of bainitic steels by changing the end of rolling temperature and the end of accelerated cooling temperature.
- The most suitable morphology for cold forming is that characterized by small and uniformly distributed MA particles in the bainitic ferrite matrix. This morphology is obtained for higher finishing rolling temperature and higher end of accelerated cooling temperature.
- The lower temperature of the last deformation (800°C) gives the larger contribution of the alotrimorphic ferrite and the strength of these samples is lower that those with the last deformation temperature of 980°C.
- Ferritic transformation of the deformed austenite is faster than that for the fully recrystallized austenite. Opposite influence was observed for the bainitic transformation.
- Modified JMAK model with the coefficients identified on the basis of dilatometric tests describes with good accuracy kinetics of phase transformation for bainitic steel.
- Good predictive capability of the conventional microstructure evolution model was confirmed by comparison of physical and numerical simulations of rod rolling.

ACKNOWLEDGEMENTS

Financial assistance of the MNiSzW, project no. R07 0006 10, is acknowledged.

REFERENCES

Avrami, M., 1939, Kinetics of phase change I, *J. Chem. Phys.*, 7, 1103-1112.

Bhadeshia, H.K.D.H., Edmonds, D.V., 1980, The mechanism of bainite formation in steels, *Acta Metallurgica*, 28, 1265-1273.

Davenport, S.B., Silk, N.J., Sparks, C.N., Sellars, C.M., 1999, Development of constitutive equations for the modelling of hot rolling, *Materials Science and Technology*, 16, 1-8.

Hansel, A., Spittel, T., 1979, *Kraft- und Arbeitsbedarf Bildsamer Formgebungs-verfahren*, VEB Deutscher Verlag fur Grundstoffindustrie, Leipzig.

Hon, K.K.B., Xu, S., 2007, Impact of product life cycle on manufacturing systems reconfiguration, *Annals of the CIRP*, 56, 455-458.

Karjalainen, L.P., Perttu, J., 1996, Characteristics of static and metadynamic recrystallization strain accumulation in hot deformed austenite as revealed by stress relaxation method, *ISIJ International*, 36, 729-736.

Kowalski, B., Sellars, C.M., Pietrzyk, M., 2000, Development of a computer code for the interpretation of results of hot plane strain compression tests, *ISIJ International*, 40, 1230-1236.

Kusiak, J., Thompson, E.G., 1989, Optimization techniques for extrusion die shape design, Proc. NUMIFORM'89, eds, Thompson, E.G., Wood, R.D., Zienkiewicz, O.C. and Samuels-son, A., Fort Collins, 569-574.

Kuziak, R., Pidvysots'kyy, V., Węglarczyk, S., Pietrzyk, M., 2011, Bainitic steels as alternative for conventional carbon-manganese steels in manufacturing of fasteners - simulation of production chain, *Computer Methods in Materials Science*, 11, 443-462.

Legwand, A., Perzyński, K., Madej, Ł., Pietrzyk, M., 2014, Approach for an automatic optimisation of production chain as a tool for intelligent manufacturing in metal forming, *Computer Methods in Materials Science*, 14 (1), 64-74.

Madej, L., Weglarczyk, S., Rauch, L., Pietrzyk, M., 2008, Modelling of production chains as a tool for intelligent manufacturing in metal forming, *Journal of Machine Engineering*, 8, 33-42.

Pereira, J., Paulre, B., 2001, Flexibility in manufacturing systems: a relational and a dynamic approach, *European Journal of Operational Research*, 130, 70-82.

Pietrzyk, M., Madej, L., Weglarczyk, S., 2008, Tool for optimal design of manufacturing chain based on metal forming, *The CIRP Annals*, 57/1, 309-312.

Szeliga, D., Gawąd, J., Pietrzyk, M., 2006, Inverse analysis for identification of rheological and friction models in metal forming, *Computer Methods in Applied Mechanics and Engineering*, 195, 6778-6798.

Waengler, S., Kawalla, R., Kuziak, R., 2008, High strength–high toughness bainitic steels alloyed with niobium for long products, *Steel Research International,* 79, spec. ed. Metal Forming Conf., 2, 273-279.

STALE BAINITYCZNE JAKO ALTERNATYWA DLA KONWENCJONALNYCH STALI WĘGLOWO-MANGANOWYCH W WYTWARZANIU ELEMENTÓW ZŁĄCZNYCH – SYMULACJA CYKLU PRODUKCJI

Streszczenie

Celem pracy było przeprowadzenie weryfikacji modeli reologicznych i modeli rozwoju mikrostruktury stosowanych w optymalizacji wytwarzania elementów złącznych ze stali bainitycznych. Wykonano symulacje fizyczne poszczególnych doświadczeń i przeprowadzono identyfikację współczynników w modelach. Szczególny nacisk położono na walcowanie na gorąco prętów i kontrolowane chłodzenie. Fizyczną symulację procesów termomechanicznych wykonano na symulatorze Gleeble 3800 i na tej podstawie wykonano identyfikację modelu rozwoju mikrostruktury. Próby dylatometryczne wykorzystano do weryfikacji modelu przemian fazowych. Do analizy mikrostruktur wykorzystano mikroskopię optyczną i elektronową. Wyniki analizy potwierdziły dobrą dokładność modeli.

Received: December 10, 2013
Received in a revised form: December 19, 2013
Accepted: December 20, 2013